P1C.1

Error Covariance Estimation for Doppler Wind Data Assimilation

Qin Xu*, National Severe Storms Laboratory, Norman OK
Leilei Wang, and Kang Nai, CIMMS, University of Oklahoma, Norman OK

1. Introduction

To optimally assimilate Doppler radar radial-velocity observations into a background wind field, it is necessary to know their error covarinaces. This study concerns how to estimate these error covariances from Doppler radial-wind innovation (observation minus background) data. This problem is to be solved by reformulating the innovation method of Xu and Wei (2001, referred to as XW) based on the non-isotropic form of radial-velocity error covariance (Xu and Gong 2003, referred to as XG). In the conventional innovation method, the observation (measurement plus sampling) errors are assumed to be non-correlated in the horizontal. This assumption is relaxed so that error correlations between neighborhood gates can revealed and assessed for the observed radial velocities.

2. Non-isotropic error covariance for v_r

Denote by $\mathbf{v} = (u, v)^T$ a two-dimensional random vector field which is Gaussian unbiased (or bias-removed), homogeneous and isotropic in the horizontal, where $(\bullet)^T$ is the transpose of $(\bullet)$. The covariance of $\mathbf{v}$ is a second-order tensor defined by $\mathbf{C_{vv}} = \langle \mathbf{v}_1 \mathbf{v}_2^T \rangle$, where $\langle(\bullet)\rangle$ denotes the expectation (ensemble mean) of $(\bullet)$ and the subscript $(\bullet)_i$ denotes the value of $(\bullet)$ at point $\mathbf{x}_i = (x_i, y_i)$ for i = 1, 2. When the coordinate system is rotated by $\alpha = \tan^{-1}[(y_2 - y_1)/(x_2 - x_1)]$, the x-axis fits into the direction of $\mathbf{r} = \mathbf{x}_1 - \mathbf{x}_2$ and the covariance tensor becomes diagonal with its two diagonal elements given by $C_{ll} = \langle l_1 l_2 \rangle$ and $C_{tt} = \langle t_1 t_2 \rangle$. Here, l_i and t_i are the two components of $\mathbf{v}_i$ (i = 1, 2) in the rotated coordinates (see Fig. 1 of XG). Under the assumed homogeneity and isotropy, C_{ll} and C_{tt} are functions of $r = |\mathbf{r}|$ only (see appendix of XW).

The covariance function of v_r is defined by $C_{vr} = \langle v_{r1} v_{r2} \rangle$, where $v_{ri} = u_i \cos\beta_i + v_i \sin\beta_i$ is the radial component of $\mathbf{v}_i = (u_i, v_i)$ (i = 1, 2) viewed from the radar, and $\beta_i = \tan^{-1}(y_i/x_i)$ (for i = 1, 2). As shown in XG, this definition leads to

$$C_{vr} = 0.5(C_+ \cos\beta_- + C_- \cos\beta_+), \tag{1}$$

where $C_+ = C_{ll} + C_{tt}$, $C_- = C_{ll} - C_{tt}$, $\beta_- = \beta_1 - \beta_2$ and $\beta_+ = \beta_1 + \beta_2 - 2\alpha$. As shown in (1), C_{vr} depends on the function forms of $C_{ll} = C_{ll}(r)$ and $C_{tt} = C_{tt}(r)$, while the latter are largely characterized by their respective decorrelation length scales [see (5.5) of XW] and ranges of correlation.

* *Corresponding author address:* Qin Xu, NSSL/NOAA, 1313 Halley Circle, Norman, OK 73069; e-mail: Qin.Xu@nssl.noaa.gov.

3. Partition of innovation covariance

Denote by v_{ri}^o the observed radial velocity at point $\mathbf{x}_i$ (on the conical surface at the lowest tilt of radar scans) and by v_{ri}^b the background radial velocity interpolated to point $\mathbf{x}_i$. Denote by $v_{ri}^{o\prime}$ the error in v_{ri}^o and by $v_{ri}^{b\prime}$ the error in v_{ri}^b. The associated observation and background error covariances are defined by $C_{vr}^o = \langle v_{r1}^{o\prime} v_{r2}^{o\prime} \rangle$ and $C_{vr}^b = \langle v_{r1}^{b\prime} v_{r2}^{b\prime} \rangle$, respectively. The radial-velocity innovation at point $\mathbf{x}_i$ is defined by $v_{ri}^d = v_{ri}^o - v_{ri}^b = v_{ri}^{o\prime} - v_{ri}^{b\prime}$. Assume that $v_{ri}^{o\prime}$ is independent of $v_{ri}^{b\prime}$, then the innovation covariance can be partitioned as follows

$$\langle v_{r1}^d v_{r2}^d \rangle = \begin{cases} C_{vr}^b & \text{for } r \ge r_o \\ C_{vr}^o + C_{vr}^b & \text{for } r < r_o, \end{cases} \tag{2}$$

where r_o is the range of correlation for the observation (measurement plus sampling) error $v_{ri}^{o\prime}$. Based on the structure of the computed innovation covariances near r = 0, r_o is set to 2 km (see Fig. 2).

The background error covariance C_{vr}^b can be modeled by (1) with C_+ and C_- expressed by the truncated spectral expansions in (4.1) of XW, but the range of correlation for the background error is now set to D = 100 km based on the overall structure of the computed innovation covariances (up to r = 250 km). The background radial-wind error covariance can be estimated by fitting the spectral expansion of C_{vr}^b to the innovation covariances computed according to (2) over the range of $r_o \le r \le D$. By extracting the estimated C_{vr}^b from the innovation covariances, the residuals of the fitting can be used to estimate the observation error variance at r = 0 and observation error covariance over the range of $0 \le r \le r_o$.

4. Data description

The radial-velocity observations used in this study were collected from the terminal Doppler weather radar (TDWR) at the Oklahoma City airport for the period from 0601 to 1857 UTC on 26 October 2002. The weather was calm during this period and the data coverage was within 88.8 km from the radar. The data were scanned every 5 minutes per volume with high spatial resolutions: 150 m in the radial direction and around 1^o in the azimuthal direction. The scans at the lowest tilt (0.3^o) are treated as horizontal and used to compute the innovations. After dealiasing and quality control, 45 fields of radial-velocity observations are selected to generate the innovation fields.

The background vector velocity fields were produced by the two-dimensional Doppler wind analysis package (Liu et al. 2003) running real-time with input radial-velocity data from KTLX radar. The domain is 120x120 km^2 on a 81x81 grid (Δx = 1.5 km) centered at the KTLX site on the conical surface of the lowest tilt (0.5^o) of radar scans. The background vector velocities are interpolated horizontally to the observation locations in the overlapped area within 88 km radial distance from TDWR (Fig. 1) and then projected onto the TDWR beam directions to obtained the background radial velocities. Vertical distances between the observation points (at the conical surface of the lowest tilt of TDWR scans) and the interpolated background data points (at the conical surface of the lowest tilt of KTLX scans) are smaller than 0.5 km and thus neglected.

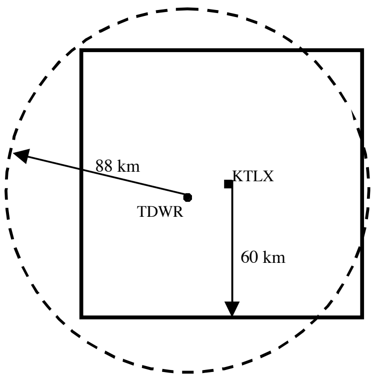

Fig. 1. Coverage (dashed circle) of TDWR observations and domain (solid square) of background field produced from KTLX observations.

5. Innovation covariance fitting and results

From the 45 fields of radial-velocity observations, 45 innovation fields are generated to compute the innovation covariances according to (2). The innovation covariances are binned every 250 m in r and every 0.1 in $\cos\beta_-$ and $\cos\beta_+$. The background error covariance functions are estimated by fitting the spectral expansion of C_{vr}^b [obtained by substituting (4.1) of XW into (1)] to the binned innovation covariances over $r_o \le r \le D$.

Examples of the binned innovation covariances are shown in Fig. 2. The estimated background error covariance functions are shown in Fig. 3 for $0 \le r \le 0.5D$ = 50 km. Beyond 50 km, the estimated covariance functions decrease slowly and smoothly to D = 100 km (not shown). The innovation variance is 13.1 m^2s^{-2} (not shown), which is the sum of the background and observation error variances. The background error variance is $C_+(0)$ = 7.3 m^2s^{-2} as estimated by the vertical interception of $C_+(r)$ at r = 0 in Fig. 3. The observation error variance is thus given by 5.8 m^2s^{-2}.

The thin-solid curve in Fig. 2 is binned in the 0.05 vicinities of $\cos\beta_-$ = 1.0 and $\cos\beta_+$ = -1.0 which gives $C_{vr} = C_{tt}$ according to (1). This curve is thus largely fitted, as it should be, by the estimated C_{tt} in Fig. 3 over the range of $r_o \le r \le D$ according to (2). Similarly, the dotted and thick-solid curves in Fig. 3 are largely fitted by the estimated C_{ll} and $0.5C_+$, respectively.

As r decreases into the range of $r < r_o$ (= 2 km), all the three curves in Fig. 2 start to increase rapidly, indicating that the observation errors are correlated between neighborhood gates within the range of $r < r_o$. The difference between the thin-solid (or dotted) curve in Fig. 2 and the estimated C_{tt} (or C_{ll}) in Fig. 3 represents the observation error covariance C_{tt}^o (or C_{ll}^o) in the range of $0 \le r < r_o$.

Using (4.5) of XW, C_+ is partitioned. The divergent part is found larger than the rotational part (Fig. 3). In comparison with the results in Fig. 6 of XW, the enhanced divergent part is dynamically consistent with the reduced scale (from synoptic to mesoscale).

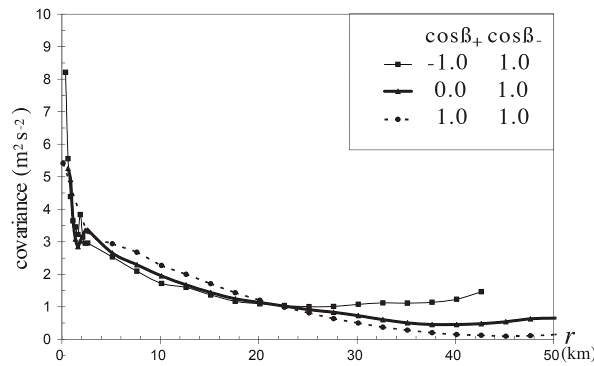

Fig. 2. Binned innovation covariances.

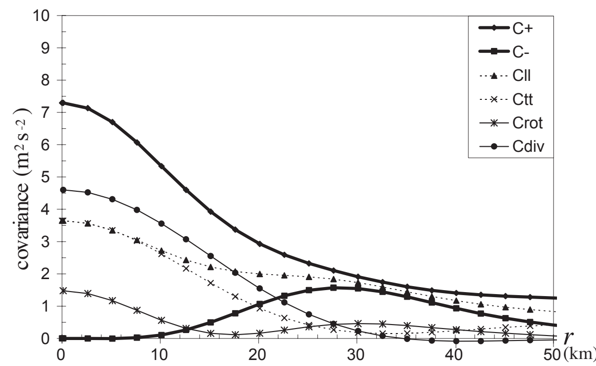

Fig. 3. Estimated background error covariance functions.

Acknowledgments. The research work was supported by the NOAA A8R2WRP project, by the FAA contract IA# DTFA03-01-X-9007 to NSSL, and by the ONR Grant N000140310822 to the University of Oklahoma.

References

Xu, Q., and J. Gong, 2003: Background error covariance functions for Doppler radial-wind analysis. *Quart. J. Roy. Meteor. Soc.*, **129**, 1703-1720.

Xu, Q., and L. Wei, 2001: Estimation of three-dimensional error covariances. Part II: Analysis of wind innovation vectors. *Mon. Wea. Rev.*, **129**, 2939-2954.

Liu, S., P. Zhang, L. Wang, J. Gong, and Q. Xu, 2003: Problems and solutions in real-time Doppler wind retrievals. P3C.5 in this volume.